

Computational Investigation of Technetium(IV) Incorporation into Inverse Spinels: Magnetite (Fe_3O_4) and Trevorite (NiFe_2O_4)

Frances N. Smith,[†] Wooyong Um,^{*,†,¶} Christopher D. Taylor,^{‡,§} Dong-Sang Kim,[†] Michael J. Schweiger,[†] and Albert A. Kruger^{||}

[†]Pacific Northwest National Laboratory, 902 Battelle Boulevard, Richland, Washington 99354, United States

[¶]Pohang University of Science and Technology (POSTECH), Pohang, South Korea

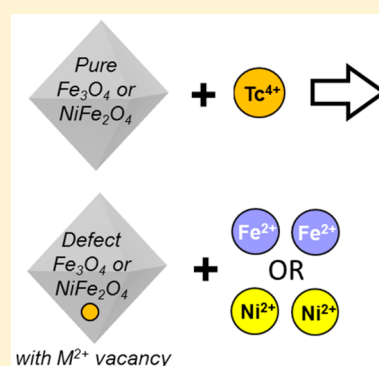
[‡]Fontana Corrosion Center, Materials Science and Engineering, The Ohio State University, Columbus Ohio 43210, United States

[§]Strategic Research and Innovation, DNV GL, Dublin Ohio 43017, United States

^{||}United States Department of Energy, Office of River Protection, P.O. Box 450, Richland, Washington 99352, United States

Supporting Information

ABSTRACT: Iron oxides and oxyhydroxides play an important role in minimizing the mobility of redox-sensitive elements in engineered and natural environments. For the radionuclide technetium-99 (Tc), these phases hold promise as primary hosts for increasing Tc loading into glass waste form matrices, or as secondary sinks during the long-term storage of nuclear materials. Recent experiments show that the inverse spinel, magnetite [$\text{Fe(II)Fe(III)}_2\text{O}_4$], can incorporate Tc(IV) into its octahedral sublattice. In that same class of materials, trevorite [$\text{Ni(II)Fe(III)}_2\text{O}_4$] is also being investigated for its ability to host Tc(IV). However, questions remain regarding the most energetically favorable charge-compensation mechanism for Tc(IV) incorporation in each structure, which will affect Tc behavior under changing waste processing or storage conditions. Here, quantum-mechanical methods were used to evaluate incorporation energies and optimized lattice bonding environments for three different, charge-balanced Tc(IV) incorporation mechanisms in magnetite and trevorite (~5 wt % Tc). For both phases, the removal of two octahedral Fe(II) or Ni(II) ions upon the addition of Tc(IV) in an octahedral site is the most stable mechanism, relative to the creation of octahedral Fe(III) defects or increasing octahedral Fe(II) content. Following hydration-energy corrections, Tc(IV) incorporation into magnetite is energetically favorable while an energy barrier exists for trevorite.



INTRODUCTION

At locations around the world where nuclear materials are stored or have been processed, certain radioactive isotopes require long-term monitoring or novel storage solutions due to their persistence, radiotoxicity, or mobility in the environment. The radioisotope technetium-99 (Tc), with its long half-life (2.1×10^5 years) and relatively high thermal fission yield (~6%),¹ is a radiological risk driver² due to its enhanced mobility in the environment as the oxidized pertechnetate anion (Tc(VII)O_4^-).^{3,4} For example, at the Hanford Site in south central Washington State, up to 55 million gallons of radioactive waste from nuclear materials processing activities are stored in 177 underground tanks awaiting solidification in glass waste forms.⁵ Of that stored waste, approximately 1.5×10^3 kg is Tc.⁶ Due to its high volatility at elevated temperatures, unique methods are needed to effectively capture and increase Tc retention when generating glass waste forms.⁶ Additionally, the release of legacy waste into the surrounding environment over the decades since it was produced⁵ has led to significant research efforts focused on the interaction of Tc (usually as Tc(VII)O_4^-) with mineral phases commonly found in the subsurface, such as iron oxides and oxyhydroxides, often in the presence of Fe(II) as a reductant.^{2-5,32-36}

Iron oxides and oxyhydroxides fulfill a number of roles in minimizing radionuclide mobility in the environment. Due to their ubiquity in natural and man-made environments, diverse structures, and reactive surfaces, these phases are useful in a variety of industrial and scientific applications.⁷ In the context of this study, iron oxides and oxyhydroxides can serve as (1) primary hosts or waste forms that incorporate radionuclides directly into their structures;⁸⁻¹² (2) carrier phases that increase radionuclide stability and waste loading in other waste forms (e.g., borosilicate glasses);¹²⁻¹⁵ and (3) phases that exist in nature, or readily form due to the corrosion of iron-bearing materials, that act as sinks by participating in reactions that minimize radionuclide mobility.^{10,16-19} The work described herein focuses specifically on the role of carrier phases, aiming to determine favorable charge-compensation mechanisms by which inverse spinel-structured iron oxides, magnetite [$\text{Fe(II)-Fe(III)}_2\text{O}_4$] and trevorite [$\text{Ni(II)Fe(III)}_2\text{O}_4$], incorporate technetium as Tc(IV) into their structures.

Received: January 13, 2016

Revised: April 4, 2016

Accepted: April 5, 2016

Published: April 5, 2016

Magnetite and trevorite form in a variety of natural and manmade environments. In nature, both minerals form under a wide-range of geological conditions, with magnetite being more common than trevorite.^{20,21} Due to anthropogenic processes, small particles of magnetite and trevorite are observed in the environment surrounding smelting facilities.²² Both phases have also been identified in nuclear facilities due to the corrosion of stainless steel structures outside reactor pressure vessels.²³ Finally, during the formation of glass waste forms for nuclear materials, spinel minerals have been identified as relatively stable precipitates;^{13–15} thus, leading to interest in those phases as carriers to stabilize Tc and increase waste loading.^{12,24} Interest in comparing the behavior of magnetite and trevorite as hosts for Tc comes from studies demonstrating that the addition of divalent cations (e.g., Ni(II)) into pure magnetite up to 1 wt % has been shown to make the modified magnetite more resistant to maghematisation (i.e., magnetite oxidation to maghemite, γ -Fe₂O₃) (ref 11 and references therein). Also, the addition of divalent cations, such as Co(II), to magnetite can alter phase-change transition temperatures,²⁵ which could help maintain phase stability under waste processing conditions.

Materials with the inverse spinel structure cover a wide variety of chemical compositions and are known to accommodate substituents. Magnetite and trevorite have the general formula AB₂O₄, where A represents divalent cations and B represents trivalent cations. Following the convention of O'Neill and Navrotsky,²⁶ where parentheses () and brackets [] represent tetrahedral and octahedral sites respectively, inverse spinels can be written as (B)[A₂B]O₄ where B cations occupy all of the tetrahedral sites and half of the octahedral sites, and A cations occupy the other half of the octahedral sites. In normal spinels, for comparison, all divalent cations (A) occupy the tetrahedral sites and all trivalent cations (B) occupy the octahedral sites (i.e., (A)[B]₂O₄).²⁶ For magnetite and trevorite, A represents Fe(II) and Ni(II), respectively, and B represents Fe(III) for both phases. Structurally, magnetite and trevorite are very similar since both are cubic crystals with space group symmetry 227 (*Fd* $\bar{3}m$), leaving 1/8 of the tetrahedral and 1/2 of the octahedral sites unoccupied.²⁷ Magnetite has slightly larger lattice parameters (8.394 Å)²⁸ than trevorite (8.337 Å)²⁹ due to the presence of Fe(II) which has a larger crystal radius than Ni(II) (e.g., Fe(II)_{oct} = 0.920 Å; Ni(II)_{oct} = 0.830 Å; Fe(III)_{oct} = 0.785 Å).³⁰ Given the range of elements that can be accommodated into the inverse spinel structure, Tc(IV)_{oct} with its crystal radius of 0.785 Å, should theoretically substitute well for Fe(III)_{oct} based on size alone.³⁰

While divalent, or even trivalent, substitution into these inverse spinel phases is easily charge compensated, tetravalent cation incorporation can be more challenging. In order to better understand the association of Tc with Fe(II)-bearing inverse spinel phases, recent studies have explored the incorporation of Tc into magnetite,¹¹ as well as biomagnetite.¹⁰ In Marshall et al.,¹¹ when 0.1 wt % Tc was coprecipitated with magnetite under a range of high pH values (e.g., 10–12) and analyzed using XANES and EXAFS, spectroscopic data fit well with models of Tc(IV) in octahedral coordination in the magnetite structure. Upon oxidation to form goethite or maghemite, 60–70% of the Tc was retained as Tc(IV) in the oxidized structures, suggesting that a majority of Tc(IV) in magnetite may be resistant to oxidation and release under changing environmental conditions.¹¹ Similarly, in biomagnetite samples, EXAFS data suggest a better fit for Tc(IV) in octahedral coordination with second-shell backscatter from Fe versus Tc, implying Tc(IV)

incorporation into biogenic magnetite versus a hydrous TcO₂-like phase.¹⁰

Evidence of Tc(IV) association with iron oxides and oxyhydroxides also comes from reductive adsorption experiments. For example, studies investigating the heterogeneous reduction of Tc(VII) in the presence of Fe(II) and various mineral substrates often observe Tc(IV) associated with a ferrihydrite-like phase or a Tc(IV)O₂•*n*H₂O-like phase, depending on the reacting substrates.^{31–33} In a study where Tc(VII)O₄[−] was exposed to corroded steel coupons bearing a mixture of magnetite, lepidocrocite (γ -FeOOH), goethite (α -FeOOH), and maghemite, Tc was also observed to predominantly form a mixed Tc(IV)-hydrous ferric oxide (HFO)-like precipitate (versus a TcO₂•*n*H₂O-like precipitate), when compared with X-ray spectroscopy standards.³⁴ In that phase, Tc(IV) appears to be in octahedral coordination but with limited cation neighbors, due to the surface-nature of the precipitate.³⁴

Despite the detailed data regarding Tc(IV) coordination in these bulk and surface phases, questions still remain as to what the charge-compensation mechanism is for the original Tc(IV) incorporation into magnetite, as well as trevorite. To explore that question further, atomic-scale modeling techniques were used to evaluate the energetics of three possible charge-compensated mechanisms for Tc(IV) substituting on octahedral lattice sites in magnetite and trevorite. Based on Eh-pH diagrams of Tc(IV) stability ranges overlapping with magnetite,¹⁸ in conjunction with experimental evidence,^{10,11,31–34} Tc(IV) is the expected oxidation state and was the focus of this study. Additionally, the ease of substituting Fe(II)_{oct} versus Tc(IV)_{oct} for Ni(II)_{oct} in trevorite and Ni(II)_{oct} versus Tc(IV)_{oct} for Fe(II)_{oct} in magnetite was evaluated, having implications for the synthesis of these materials experimentally and for the competition of ionic uptake in engineered and natural environments. Optimized bond-lengths and incorporation energies are presented for each stable case. Finally, a comparison between incorporation mechanisms for Tc(IV) in hematite, goethite, magnetite, and trevorite suggests that although similar octahedral coordination environments are favored for Tc(IV) in all the phases, charge-compensation mechanisms differ.

■ MATERIALS AND METHODS

Computational Details. The quantum-mechanical code CRYSTAL14³⁵ was used to calculate single-point and geometry-optimized energies for a variety of crystalline and molecular models. CRYSTAL14 uses a linear combination of Gaussian-type functions to describe the atomic orbitals for each element in the system, as defined by their basis sets.³⁵ In turn, symmetry-adapted Bloch functions are used to calculate the ground-state energy of the whole system, based on a linear combination of atomic orbitals.³⁵ Here, basis sets were chosen based on previous application to iron oxide and oxyhydroxide systems, both with Tc^[18,36] and without Tc.^{37–39} Basis sets include the Durand-21d41G effective core potential (ECP) for Fe³⁺ and Fe²⁺, with the Durand-41G ECP basis sets for O^{2−},³⁷ and a 21d41 electron core pseudopotential previously optimized for Tc⁴⁺ based on the Hay-Wadt large core pseudopotential.¹⁸ For Ni²⁺, two basis sets were tested (see Supporting Information (SI) Table S1). Following full-geometry optimizations, the Freyria ECP basis set⁴⁰ was chosen for its good agreement with experimental lattice parameters for NiO (+1.6%) and for consistency with other ECP basis sets used in this study (versus all-electron basis sets). The optimized geometries of magnetite and trevorite using these basis sets are shown in SI Table S2.

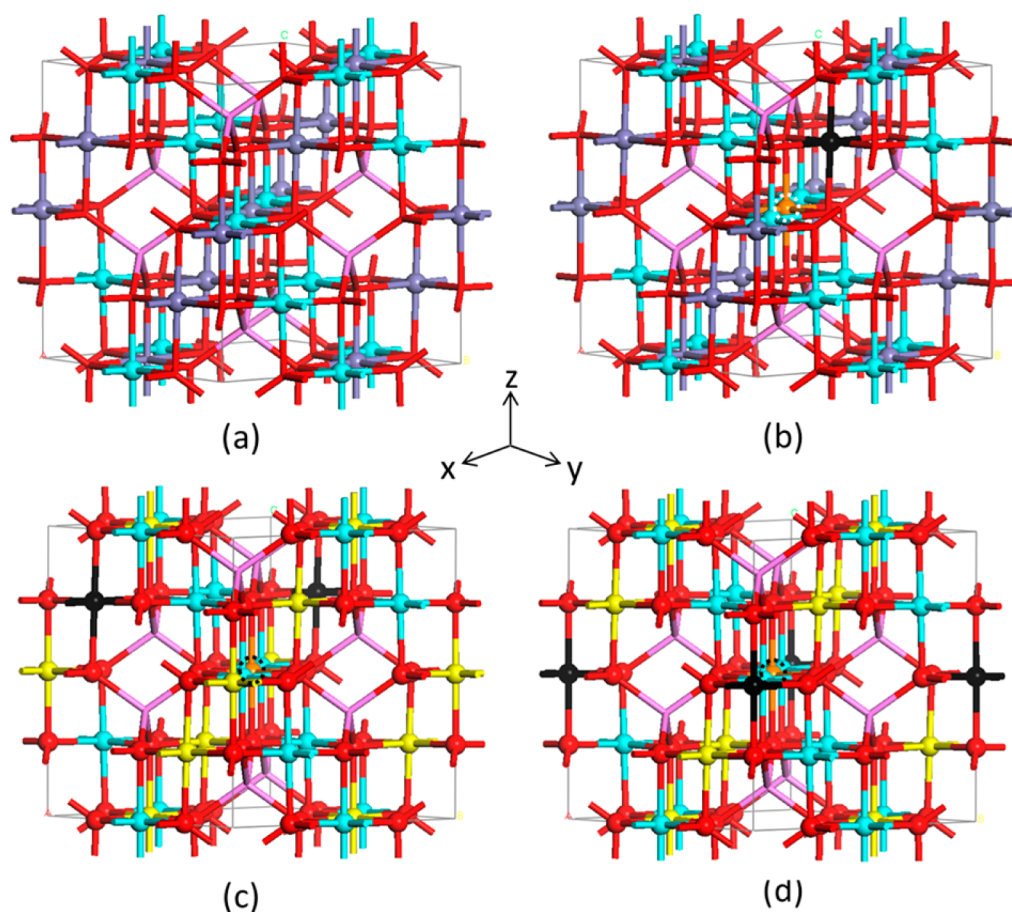


Figure 1. Ball and stick models representing (a) pure magnetite (or trevorite), and (b–d) the three stable Case 3 (M(II)-vacancy) substitution models: (b) Tc(IV) for two Fe(II)_{oct} in magnetite in the next octahedral row, nearest neighbor position (2.968 Å), (c) Tc(IV) for two Ni(II)_{oct} in trevorite in the next octahedral row, next-nearest neighbor position (5.105 Å), and (d) Tc(IV) for two Ni(II)_{oct} in trevorite in the same octahedral row (5.895 Å). Cyan spheres are Fe(III)_{oct} spin up, purple spheres are Fe(II)_{oct} spin up, yellow spheres are Ni(II)_{oct} spin up, pink lines are Fe(III)_{tet} spin down, red spheres are oxygen, orange spheres are Tc(IV)_{oct} spin up, and black spheres are vacancies. Dotted black and white circles highlight where substitutions occur. When yellow spheres are substituted for purple spheres in (a) Ni(II)_{oct} distribution in trevorite is reflected. Views are looking down the (110) crystallographic direction.

Unrestricted Hartree–Fock (UHF) computational methods were applied, which allow spin direction and density to be accounted for in magnetite and trevorite. Both phases have magnetic moments generated by the antiparallel spin alignment of metal atoms on the tetrahedral and octahedral sublattices. Specifically in magnetite, the magnetic moment arises from the net difference in spin between Fe(III)_{tet} (e.g., spin down) and Fe(II/III)_{oct} (e.g., spin up). Since there are equal numbers of Fe(III)_{tet} and Fe(III)_{oct} in magnetite, the net difference arises from the summed spin of Fe(II)_{oct}. Similarly for trevorite, the antiparallel spin for Fe(III)_{tet} and Fe(III)_{oct} cancel, leaving the summed spin of Ni(II)_{oct} as the net difference. The charge-localized behavior afforded by this UHF method is also of particular interest for magnetite, where the movement of electrons between Fe(II) and Fe(III) centers in the octahedral iron lattice induces small distortions of the surrounding crystal lattice (i.e., small-polaron behavior (ref 39 and references therein)). Even though UHF methods only account for exchange energies, unlike Density Functional Theory which approximates both exchange and correlation energies,^{41,42} UHF methods have been successful in capturing both the geometry (within 2.0–2.6%) and magnetic structure for the materials tested here (see SI Table S2). Mulliken population analysis

was used to evaluate spin density.⁴³ Additional computational details are provided in the SI.

Incorporation Energy Calculations. In the models used here, $Z = 8$ Fe₃O₄ or NiFe₂O₄ formula units (56 atoms total), corresponding to 32 O atoms, 8 Fe(III)_{tet} atoms, 8 Fe(III)_{oct} atoms, and 8 Fe(II)_{oct} or 8 Ni(II)_{oct} atoms for magnetite and trevorite, respectively (Figure 1a). The substitution of one Tc(IV) into the octahedral sublattice of magnetite (replacing two Fe(II)_{oct}) or trevorite (replacing two Ni(II)_{oct}) yields approximately 5 wt % impurity per Tc ion, whereas the substitution of one Ni(II)_{oct} for one Fe(II)_{oct} in magnetite, or vice versa for trevorite, is approximately 3 wt % impurity per ion. For comparison, these values for Tc incorporation into magnetite are higher than what is reported experimentally (e.g., 0.1 wt % Tc; Marshall et al., 2014). The next step up in cubic supercell size ($2 \times 2 \times 2$) would be $Z = 64$ or 448 atoms, yielding 0.7 wt % Tc, but these models were not pursued as part of this study due to the number of cases under initial consideration.

Here, the feasibility of atomic-scale impurity incorporation was evaluated by calculating the incorporation energy (E_{inc} ; eq 1) of different substitution reactions using the general approach:

$$E_{inc} = \sum E_{prod} - \sum E_{react} \quad (1)$$

where E_{prod} and E_{reac} refer to the summation energies of the products and the reactants in the substitution reactions outlined in eqs 2–4. For convention, a negative energy is interpreted as an energetically favorable substitution while a positive energy implies a barrier to substitution exists.

For the substitution of Tc(IV) into magnetite and trevorite, three distinct cases were tested, all involving substitutions on the octahedral sublattice as guided by experimental data for Tc(IV) in magnetite.¹¹ Case 1 is an “Fe(II) charge-balanced substitution” where an Fe(II)/Tc(IV) pair substitutes for two Fe(III)_{oct} lattice atoms in magnetite or trevorite (eq 2). Case 2 is an “Fe(III) vacancy-driven substitution” where three Tc(IV) substitute for four Fe(III)_{oct} lattice atoms in magnetite or trevorite, creating an Fe(III)_{oct} vacancy in the process (eq 3). And, Case 3 is an “M(II)-vacancy substitution” where one Tc(IV) substitutes for two lattice Fe(II)_{oct} in magnetite or two lattice Ni(II)_{oct} in trevorite, on one octahedral site, creating a divalent-cation or M(II)-vacancy in the process (e.g., eq 4).

$$E_{\text{inc}}^{\text{Fe(II)-balanced}}: E_{\text{tot}}^{\text{spinel-pure}} + nE_{\text{Tc}^{4+}} + nE_{\text{Fe}^{2+}} \rightarrow E_{\text{tot}}^{\text{spinel-defect}} + 2nE_{\text{Fe}^{3+}} \quad (2)$$

$$E_{\text{inc}}^{\text{Fe(III)-vacancy}}: E_{\text{tot}}^{\text{spinel-pure}} + 3nE_{\text{Tc}^{4+}} \rightarrow E_{\text{tot}}^{\text{spinel-defect}} + 4nE_{\text{Fe}^{3+}} \quad (3)$$

$$E_{\text{inc}}^{\text{M(II)-vacancy}}: E_{\text{tot}}^{\text{spinel-pure}} + nE_{\text{Tc}^{4+}} \rightarrow E_{\text{tot}}^{\text{spinel-defect}} + 2nE_{\text{M}^{2+}} \quad (4)$$

Additional cases were evaluated for the one-to-one substitution of Ni(II)_{oct} for Fe(II)_{oct} in magnetite (eq 5), and Fe(II)_{oct} for Ni(II)_{oct} in trevorite (eq 6). The purpose of the latter two cases was to test the ease of isovalent cation substitutions in one end-member phase versus the other for comparison with Tc(IV) incorporation energies.

$$E_{\text{inc}}^{\text{Ni(II)-sub}}: E_{\text{tot}}^{\text{mag-pure}} + nE_{\text{Ni}^{2+}} \rightarrow E_{\text{tot}}^{\text{mag-defect}} + nE_{\text{Fe}^{2+}} \quad (5)$$

$$E_{\text{inc}}^{\text{Fe(II)-sub}}: E_{\text{tot}}^{\text{trev-pure}} + nE_{\text{Fe}^{2+}} \rightarrow E_{\text{tot}}^{\text{trev-defect}} + nE_{\text{Ni}^{2+}} \quad (6)$$

In all the equations listed above, the total energies of the pure ($E_{\text{tot}}^{\text{spinel-pure}}$) and defect ($E_{\text{tot}}^{\text{spinel-defect}}$) phases of magnetite and trevorite represent calculations on solid-state crystalline phases, while the energies of individual ions (E_{ion} ; ion = Fe²⁺, Fe³⁺, Ni²⁺, and Tc⁴⁺) were performed on charged gas-phase species (see SI Table S3); n represents the number of substituting ions. No significant energy differences were observed for ionic species calculated using a cluster approach versus a periodic boundary calculation approach. “Defect” phases are ones that have been substituted with Tc(IV) or M(II) cations.

It is important to note that eqs 2–6 represent simplified systems relative to what would be expected under experimental conditions, where substituents would likely be introduced as aqueous species, and in some cases, as more oxidizing and soluble species (e.g., Tc(VII)O₄[−]). To account for these conditions, hydration-energy corrections based on experimental databases can be applied to the gas-phase reference energies of the ions, according to the method outlined in Smith et al.³⁶ A stepwise explanation of the hydration-energy correction factor and its application to calculating E_{inc} is provided in the SI Table S4 and associated discussion.

RESULTS AND DISCUSSION

Tc(IV) Substitution in Magnetite and Trevorite. Three cases for incorporation of Tc(IV) into the octahedral sublattice of magnetite and trevorite were considered: Case 1) a direct Tc(IV)–Fe(II) charge-balanced substitution (SI Figure S1); Case 2) an Fe(III)-vacancy driven substitution (SI Figure S2); and Case 3) an M(II)-vacancy driven substitution, where M is Fe or Ni (Figure 1). For each case, two to four different distributions of Tc(IV) relative to the charge-balancing mechanisms were evaluated. In all instances, single-point energy (SPE) calculations were used to evaluate whether the assigned spin densities and charge distributions were maintained for the Tc(IV)-substituted models. For stable results, where spin distributions representing Tc(IV), Fe(II), Fe(III), and Ni(II) were maintained, the single-point energy wave function was used as a “wave-function guess” to perform atom-only and full-geometry optimizations. For all other cases, Mulliken spin distributions were captured in the SI Table S5, but higher-level calculations were not pursued. Due to reference phases being gas-phase ions of specific charges, it was assumed that incorporation energies are most accurate and comparable between different cases when systems retain the assigned spin density (e.g., three unpaired spins to represent Tc(IV); two unpaired spins for Ni(II)); however, even in cases where the starting spin density was not maintained, insight can be gained into the stability of the proposed charge compensation mechanisms.

Broadly speaking, stabilizing Tc(IV) in magnetite and trevorite proved difficult for all charge-compensation cases tested, except for one. For example, Fe(II)-charge-balanced substitutions of Tc(IV) for two Fe(III)_{oct} in magnetite (Case 1) led to the oxidation of Tc to Tc(V) or Tc(VI), accompanied by the oxidation of two Fe(II)_{oct} to Fe(III)_{oct} (SI Table S5; Figure S2). These results suggest that the addition of excess Fe(II)_{oct} to the system along with Tc(IV) is not stable in unit cells of this size without further oxidation of Tc. For trevorite, one arrangement of Tc(IV) and Fe(II) for two Fe(III)_{oct} led to the stabilization of Tc(IV); however, Ni(II) was reduced to Ni(I) at the expense of the excess Fe(II)_{oct} (SI Table S5; Figure S2). The other arrangement of defects in Case 1 led to the oxidation of Tc(IV) to Tc(V) and Fe(II)_{oct} to Fe(III) while Ni(II) remained stable (SI Table S5; Figure S2). In trevorite, the addition of excess Fe(II)_{oct} to stabilize Tc(IV) also leads to oxidation and reduction of Ni as well as Tc in this sized model.

For Case 2, where three Tc(IV) substituted for four Fe(III)_{oct} creating a vacancy in the process, spin distributions were highly variable in magnetite and trevorite. Specifically, in magnetite, spin flipping of the unpaired spins in Tc(IV) occurred, as well as Tc reduction to Tc(II) or Tc(0). These highly variable results were attributed to high defect loading in a unit cell of this size (e.g., 15 wt % Tc total; 5 wt % per Tc) and results were deemed unphysical due to this behavior (SI Table S5; Figure S2). In trevorite, Tc oxidation states ranged from Tc(III) to Tc(VI) and some Ni(II) spin densities were compromised (e.g., oxidized to Ni(III) or Ni(IV)) suggesting that Tc waste loading might be too high in this unit cell, as well (SI Table S5; Figure S2). While these results do not rule out this substitution mechanism, they do imply that it is not likely for high waste loading scenarios. For Cases 1 and 2, it should be noted that all the “spin contamination” occurred on the octahedral sublattice rather than the tetrahedral sublattice in both inverse spinels since the expected spin for Fe(III)_{tet} was always maintained. In this regard, results are consistent with

dominant charge mobility on the octahedral sublattice of inverse spinels.^{44,45}

For the unit cells tested, the creation of M(II)-vacancies (Case 3) in magnetite and trevorite led to the most instances of expected spin density being maintained. For Tc(IV) substitution into pure end-member magnetite (Figure 1a), one configuration out of three tested was stable. Figure 1b shows the stable configuration where the Fe(II)_{oct} vacancy was in the next octahedral layer above the Tc(IV) substitution in a nearest-neighbor location separated by 2.968 Å. The other two cases tested resulted in “spin contamination” (SI Table S5a), where Tc was oxidized to Tc(V) or Tc(VI) depending on the spacing of defects, and lattice Fe(II)_{oct} was oxidized to Fe(III)_{oct} in the process. For trevorite (Figure 1a), two out of the three configurations tested were stable for Case 3 (SI Table S5b). In Figure 1c, the Ni(II)_{oct} vacancy was one octahedral layer above the Tc(IV)_{oct} substituent in a next-nearest neighbor location separated by 5.105 Å. In Figure 1d, Tc(IV)_{oct} and the Ni(II)_{oct} vacancy were in the same (110) row, separated by 5.895 Å. For the case where Tc(IV)_{oct} was not stable, it was reduced to Tc(III) (SI Table S5b) and excess spin was likely accommodated by oxygen spin densities, especially near the vacancy. While these models would likely benefit from larger supercells to lower Tc loading and allow for additional options for defect arrangements, more detailed comparisons will be made of the three Case 3 scenarios where Tc(IV)_{oct} remained stable in the remainder of this section.

In order to evaluate the relative stability of Tc(IV) in magnetite versus trevorite, a comparison of incorporation energies is necessary. Incorporation energies for the three spin-stable cases are presented in Table 1. In these cases, the E_{inc} values are

Table 1. Full-Geometry Optimized Total and Incorporation Energies for Magnetite and Trevorite^a

| model | opt. ^b | E_{tot}^{spinel} (Ha) | E_{tot}^{spinel} (eV) | E_{inc} (Ha) | E_{inc} (eV) | $E_{inc-hyd}$ (eV) |
|---------------------------|-------------------|-------------------------|-------------------------|----------------|----------------|--------------------|
| (a) magnetite (pure) | FG | -1018.70 | -27 719.79 | | | |
| (a) trevorite (pure) | FG | -2194.95 | -59 726.75 | | | |
| (b) case 3-Mag (2.968 Å) | FG | -987.44 | -26 869.13 | -1.55 | -42.2 | -1.33 |
| (c) case 3-Trev (5.105 Å) | FG | -1869.57 | -50 872.96 | -1.25 | -33.96 | 4.00 |
| (d) case 3-Trev (5.895 Å) | FG | -1869.60 | -50 873.68 | -1.27 | -34.67 | 3.29 |
| Ni(II)-doped Magnetite | FG | -1165.73 | -31 720.63 | -0.12 | -3.40 | -0.49 |
| Fe(II)-doped trevorite | FG | -2047.92 | -55 725.63 | 0.13 | 3.47 | 0.56 |

^aNote: Letters (a–d) correspond to Figure 1; values in parentheses are Tc(IV)-M(II)-vacancy distances. ^bOptimization parameters: FG = full geometry.

negative when referenced against gas-phase ions (eq 2–4), suggesting that Tc(IV) incorporation is energetically favorable. Here, Tc(IV) incorporation into magnetite is approximately 7–8 eV more favorable than into trevorite for the full-geometry optimized cases. Looking at trevorite alone, cases vary only by 0.7 eV depending on where the defect is relative to the Tc(IV) ion in the structure. The longer distance between Tc(IV) and the Fe(II)_{oct}-vacancy in trevorite is favored over the shorter distance. In all cases, however, E_{inc} values for magnetite and trevorite are larger than would be expected under experimental

conditions due to reference phases being gas-phase ions rather than hydrated ions.⁴⁶

To explore the effect of gas-phase versus hydrated reference species, a correction factor was applied following the method described in Smith et al.³⁶ Details of that correction factor are presented in the SI (Table S4), where the calculated ionic gas-phase energies are related back to relevant aqueous species in a stepwise fashion by drawing upon experimentally known energies for each step. Hydration-energy corrected incorporation energies ($E_{inc-hyd}$) are shown in the far-right column of Table 1. For the full-geometry optimized cases, Tc(IV) incorporation in magnetite is still energetically favorable, although the $E_{inc-hyd}$ is significantly smaller than for the gas-phase reference case (approximately -1 eV versus -42 eV). In contrast, the $E_{inc-hyd}$ becomes positive (e.g., 3–4 eV) for Tc(IV) incorporation into trevorite, suggesting that there is an energy barrier to Tc(IV) incorporation at low temperature. It is important to note that while the calculations themselves take place at 0 K, the experimental energies adjust values toward ambient temperatures (SI Table S4 and associated discussion). In trevorite, the hydration energy correction still favors the longer distance between Tc(IV) and the Fe(II)_{oct}-vacancy with a smaller, albeit positive $E_{inc-hyd}$ value.

A useful measure of comparison between theory and experiment is bond lengths. Overall, lattice parameters of all full-geometry optimized magnetite and trevorite cases lengthen by 2–2.5% with respect to experimental data (SI Table S2), attributed to basis set performance. Focusing on local coordination environments, an average of six optimized < Fe–O>, < Ni–O>, and < Tc–O> bond lengths are shown in Table 2 for pure end-member magnetite and trevorite, as well as the three stable substitution configurations. For comparison, starting bond-lengths (SPE) and fully geometry optimized bond lengths (FG) are shown. Looking at < Fe(II)-O> versus < Fe(III)-O> bond-lengths in pure and Tc-substituted magnetite, the ~0.1 Å difference in octahedral coordination is consistent with differences in averaged crystallographic radii data (0.135 Å).³⁰ Additionally, < Fe(III)-O> bond lengths in pure trevorite are ~0.05 Å shorter than < Ni(II)-O> bond lengths, consistent with an estimated 0.045 Å difference in crystal radii.³⁰ These results suggest that the models are accurately capturing the differences in cation bonding environments in these phases. Optimized magnetite exhibits longer average < Tc–O> bond lengths than trevorite, attributed to its larger unit cell (0.68% from experimental data).^{16,17} The case where the Tc(IV)–Ni(II)-vacancy distance is shorter in trevorite (c) leads to < Tc–O> bonds only 0.3% shorter than Tc(IV)_{oct} in magnetite. In contrast, when the Tc(IV)–Ni(II) vacancy distance is greater in trevorite (d), greater < Tc–O> bond length contraction is observed (e.g., 4.8% shorter than in magnetite), suggesting that defect spacing has an effect on local coordination environments.

Comparisons can be made with experimental data for < Tc–O> bond lengths in TcO₂⁴⁷ and Tc coprecipitated with magnetite.^{4,5} In TcO₂, < Tc–O> bond-lengths for Tc(IV) in octahedral coordination average 1.98 Å.⁴⁷ For calculated Tc(IV) in magnetite, < Tc–O> bond-lengths are 0.08 Å longer for the FG case. In trevorite, < Tc–O> bond-lengths range from 0.03 Å shorter to 0.06 Å longer for the FG cases, depending Tc(IV)–Ni(II)-vacancy spacing. Both these cases suggest that the octahedral bonding environment in the inverse spinels are fairly consistent with Tc(IV) in TcO₂. For comparison with experimental data suggestive of Tc(IV) incorporation into magnetite based on EXAFS,¹¹ < Tc–O> bond-lengths

Table 2. Starting and Optimized Bond Lengths for Fe-, Ni-, and Tc–O in Magnetite and Trevorite^a

| model | opt ^b | Fe(III) _{oct} -O Å | Fe(II) _{oct} -O Å | Ni(II) _{oct} -O Å | Tc(IV) _{oct} -O ^c Å |
|-------------------------------------|------------------|-----------------------------|----------------------------|----------------------------|-----------------------------------------|
| (a) magnetite (pure) ^c | SPE | 2.058 | 2.058 | | |
| (a) magnetite (pure) | FG | 2.060 | 2.143 | | |
| (a) trevorite (pure) ^d | SPE | 2.044 | | 2.044 | |
| (a) trevorite (pure) | FG | 2.053 | | 2.107 | |
| (b) case 3-Mag (2.968 Å) | SPE | 2.058 | 2.058 | | 2.058 |
| (b) case 3-Mag (2.968 Å) | FG | 2.054 | 2.159 | | 2.046 |
| (c) case 3-Trev (5.105 Å) | SPE | 2.044 | | 2.044 | 2.044 |
| (c) case 3-Trev (5.105 Å) | FG | 2.055 | | 2.047 | 2.039 |
| (d) Case 3-Trev (5.895 Å) | SPE | 2.044 | | 2.044 | 2.044 |
| (d) Case 3-Trev (5.895 Å) | FG | 2.049 | | 2.127 | 1.952 |
| Tc in TcO ₂ ^e | Exper. | | | | 1.98 |
| Tc in magnetite ^f | Exper. | | | | 2.00 (1.99) |

^aNote: Letters (a–d) correspond to Figure 1; values in parentheses are Tc(IV)-M(II)-vacancy distances. ^bOptimization parameters; SPE = Single-point energy (starting geometry); FG = full geometry. ^cStructure after Fleet. ^dStructure after Gorter. ^eRodriguez et al. ^fValue in parentheses represents reoxidized case from Marshall et al.

(coordination number of 6) are reported at 2.00 Å for unoxidized samples and 1.99 Å for reoxidized samples (post-precipitation). Nearly identical < Tc–O > bond distances are reported for unoxidized and (re)oxidized Tc-doped, biogenic magnetite as well.¹⁰ For magnetite, calculated < Tc–O > bond-lengths are 0.05 Å longer than those reported experimentally [11], likely due to the increase in lattice parameters relative to experimental data (SI Table S2). For trevorite, the optimized < Tc–O > bond-lengths are 0.05 Å shorter or 0.04 Å longer, depending on Tc(IV)–Ni(II)-vacancy defect spacing. In general, slightly shorter < Tc–O > bonds length would be expected in trevorite relative to magnetite due to its smaller lattice parameters. Overall, calculated and experimental < Tc–O > bond lengths in magnetite and trevorite are supportive of Tc(IV) in octahedral environments versus tetrahedral environments. For comparison, experimentally determined < Fe(III)_{tet}-O > bond-lengths in magnetite and trevorite are 1.889 and 1.876 Å, respectively.^{28,29}

Additional support for the creation of M(II)_{oct} defects in magnetite and trevorite upon the addition of Tc(IV) to the structure comes from looking at the cation coordination number data for experimental Tc(IV) in magnetite, as presented by Marshall et al.¹¹ In pure end-member magnetite, each Fe_{oct} has six nearest-neighbor Fe_{oct} at 2.968 Å, and six next-nearest neighbor Fe_{tet} atoms at distances of 3.480 Å.^{11,28} In magnetite coprecipitated with Tc, the number of Fe atoms coordinating Tc(IV) under reducing conditions is 4.3 ± 1.5 for the first Fe shell at 3.04 Å (presumably Fe_{oct}), and 4.0 ± 1.4 for the second Fe shell at 3.48 Å (presumably Fe_{tet}).¹¹ Similar observations are made for Tc(IV) in magnetite oxidized for 21 days and 152 days, except that the second-Fe shell coordination is reduced to 3.6 ± 1.1 and 3.7 ± 1.2 at 3.47 Å, respectively.¹¹ For the magnetite case in this study, where Tc(IV) is separated from the Fe(II)_{oct} vacancy by 2.968 Å (Figure 1b), the reduction in first-shell Fe_{oct} nearest neighbors would be within error of experimental data, since just one Fe(II)_{oct} vacancy is created per Tc(IV) incorporated (i.e., coordination number of 5). It should be noted, however, that lower cation coordination numbers in experiments could also be indicative of Tc(IV) substituted in (near-)surface environments.⁵ While no direct experimental comparisons are available for Tc(IV) incorporation in trevorite at present, it could be hypothesized that a decrease in coordination number would be expected for increasingly removed

cation coordination shells since Ni(II)_{oct} defects appear stable beyond the first and second cation coordination shells, based on modeling results.

An important distinction between the models used here and experimental data for Tc(IV) association with iron oxides and oxyhydroxides is Tc wt % (e.g., Five wt % Tc versus 0.1 wt % Tc in magnetite¹¹). Other studies reporting Tc association with iron oxides and oxyhydroxides suggest 0.6 to 1 wt % Tc;⁴⁸ therefore, these models likely represent upper incorporation limits of Tc in magnetite, possibly exceeding that limit in trevorite (based on positive $E_{inc-hyd}$). Previous studies on Tc(IV) incorporation into hematite using larger supercells suggest that E_{inc} becomes less favorable with increasing Tc wt % between <1 and 3 wt % Tc.¹⁸ As such, it is likely that lower concentrations of Tc(IV) in magnetite and trevorite would be increasingly stable below 5 wt % Tc.

M(II) Substitution in Magnetite and Trevorite End-Members. In a real-world scenario, Tc(IV) might be in competition with Ni(II) if Ni-doped magnetites are being synthesized as “carrier phases” to increase Tc loading in waste glass, or Tc(IV) might compete with cations in solution when reductively adsorbing or coprecipitating with magnetite in the environment. To evaluate the ease of M(II) cation incorporation into each end-member phase, E_{inc} were calculated for near-endmember solid solution models (e.g., 3 wt % excess M(II) cation) for comparison with Tc(IV) incorporation energies. Specifically, one Ni(II) was substituted for one Fe(II)_{oct} in magnetite (eq 5; SI Figure S3a), and one Fe(II) was substituted for one Ni(II)_{oct} in trevorite (eq 6; SI Figure S3b). Incorporation energy results for Ni(II)-doped magnetite and Fe(II)-doped trevorite models are shown in Table 1. Results suggest it is energetically favorable to incorporate at least one Ni(II) cation into magnetite (–3.40 eV gas phase; –0.494 eV hydrated for FG cases), whereas an energy barrier exists for incorporating one Fe(II) into trevorite (3.47 eV gas phase; + 0.56 eV hydrated). When the excess enthalpy of mixing is calculated by subtracting out the ideal enthalpy of mixing between the two end-members for the full-geometry optimized cases, small, but slightly positive excess enthalpies are calculated for both cases (e.g., 0.001 eV for one Ni(II) in magnetite and 0.002 eV for one Fe(II) in trevorite; see SI Table S6 and associated discussion for details). These results are consistent with a study by Andersson and Stanek²³ where DFT methods were used to explore solid solution

energetics between a number of spinel and inverse spinel end-members. For magnetite and trevorite, solid solution energies are near zero (neither strongly favorable nor unfavorable) for one Ni(II) in magnetite and slightly higher (less favorable) for one Fe(II) in trevorite;²³ however, upon completion of the entire solid solution between magnetite and trevorite, mixing enthalpies become negative (favorable) indicating complete miscibility between the two end-members. Their results are consistent with experimental data and the occurrence of magnetite-trevorite solid solutions in nature.²¹ With respect to competitive incorporation of Tc(IV) versus M(II) cations during synthesis of inverse spinels, the more favorable $E_{\text{inc-hyd}}$ for Tc(IV) in magnetite compared with Ni(II) makes incorporation seem plausible. In contrast, Tc(IV) incorporation into trevorite might be less favorable in the presence of excess Fe(II) due to the lower energy barrier for incorporation of Fe(II) versus Tc(IV) at the wt % values explored here.

In addition to calculated incorporation energies, the relative ease of substituting Ni(II) into magnetite versus Fe(II) into trevorite may be related to cation size. This observation is consistent with reports for some solid solution systems where it is often easier to substitute a smaller cation into a larger site rather than vice versa.⁴⁹ For Ni(II)_{oct} substitution into an Fe(II)_{oct} site, the crystal radii of Ni(II)_{oct} (0.830 Å) is 0.09 Å smaller than high-spin Fe(II)_{oct} (0.920 Å);³⁰ hence, Ni(II)_{oct} substitution into magnetite would be more facile than Fe(II)_{oct} into trevorite. If the same size-driven logic applies for Tc(IV) substitution into magnetite and trevorite, even though it is not a 1:1 solid-solution substitution due to charge imbalance, Tc(IV) incorporation into magnetite Fe(II)_{oct} sites might be more favored than in trevorite given the greater difference in crystal radii between Tc(IV)_{oct} (0.785 Å) and Fe(II)_{oct} (0.920 Å) versus Tc(IV)_{oct} and Ni(II)_{oct} (0.830 Å).³⁰ If competition between Tc(IV) and Ni(II) is concerned for incorporation into magnetite, the 0.045 Å-larger crystal radius of Ni(II)_{oct} versus Tc(IV)_{oct} could make Tc(IV) more competitive. Navrotsky⁴⁹ also points out that difference in bonding character and charge of the substituting species contributes to differences in mixing energies which would also come into play here; however, these energetic contributions were not specifically evaluated here.

Trends in Tc(IV) Incorporation in Iron Oxides and Oxyhydroxides. During the processing of nuclear materials or when mineral phases are considered as radionuclide sinks in the environment, the question arises as to how stable impurities are in crystalline structures under varying conditions (e.g., temperature, Eh, pH). The apparent preference of Tc(IV) for octahedral bonding environments in different iron oxide and oxyhydroxide phases is important because of the solid state (i.e., topotactic) changes these phases go through as a function of changing conditions.^{50–54} For example, if the site hosting Tc(IV) is similar across a variety of different phases, then there may be greater opportunity to retain Tc in the structures despite changing environmental conditions (e.g., oxidative or reductive transformation) or competitive processes, like impurity diffusion, at elevated temperatures. When comparing modeling studies looking at Tc(IV) incorporation in octahedral iron sites of hematite (α -Fe₂O₃),¹⁸ goethite (α -FeOOH),³⁶ magnetite, and trevorite, the variable that appears to differ is the charge compensation mechanism. Here, the creation of vacancies and substitutions were favored on the M(II)_{oct} sites rather than on the M(III)_{oct} sites. Experimentally, when magnetite becomes oxidized to maghemite, Fe(II)_{oct} cations are essentially lost from the system leaving octahedral iron vacancies and only Fe(III)

remaining in the γ -Fe₂O₃ structure.⁵⁵ For Tc(IV) substitution in goethite,³⁶ the creation of H-vacancies is favored when referenced against gas-phase ions; however, when hydration energy corrections are applied, the creation of 4Fe(III) defects to accommodate 3Tc(IV) substituents becomes increasingly competitive (akin to Case 2 here). The loss of protons, which occurs via diffusion experimentally, parallels the transformation that occurs when goethite becomes hematite with increasing temperature.⁵⁶ In contrast, for Tc(IV) in hematite, an Fe(II) charge-balancing mechanism (herein Case 1) was found to be stable and consistent with experimental evidence for an increase in Fe(II) in hematite thin films doped with Ti(IV);⁵⁷ however, other charge compensation schemes were not analyzed in that study. In two cases out of three, the substitution of Tc(IV) in magnetite/trevorite and goethite follows a charge compensation path that parallels the natural oxidation of those phases (e.g., magnetite to maghemite or goethite to hematite) versus one where excess reductants are stabilized in the system.

Focusing on magnetite, it is important to note that the addition of other M(IV) cations to the structure (e.g., Ti(IV)) is associated with an increase in structural Fe(II). Specifically, detailed characterization of natural titanomagnetite samples from Hanford Site sediments, as well as synthesized titanomagnetite nanoparticles, point to Ti(IV) substitution into octahedral coordination sites and an increase in structural Fe(II) experimentally.^{58,59} Experimental investigations into the substitution of Sn(IV) into the magnetite structure also point to the possibility of excess Fe(II) charge-balancing Sn(IV); however, that evidence was based on X-ray diffraction data.⁶⁰ With regard to Tc(IV)-doped magnetite, Fe(II)/Fe(III) ratios measured by Marshall et al.¹¹ were hyper-stoichiometric (greater than 0.5) for one sample formed under reducing conditions, and substoichiometric for all other samples, even when measured under reducing conditions, possibly due to some percentage of goethite in the solid phases. Given the mixed observations regarding the possible charge compensations mechanisms for M(IV) doping in magnetite, further investigations are warranted to determine if the same mechanism holds true for all similarly charged species substituting on the octahedral sites, or if other factors (e.g., electrochemical) affect the stability of excess Fe(II) versus defect formation. Additional factors, such as computational model size or the ability to impart a reducing potential during optimization could also affect those results, as the latter was not captured in the models applied in this study and would be of interest in future investigations.

■ ASSOCIATED CONTENT

📄 Supporting Information

The Supporting Information is available free of charge on the ACS Publications website at DOI: 10.1021/acs.est.6b00200.

Basis set testing for NiO, additional computational details, reference phase energies, optimized geometry information for all phases considered, hydration-energy correction information, spin-distribution information, and excess enthalpy calculations for M(II) substitution and associated models (PDF)

■ AUTHOR INFORMATION

Corresponding Author

*Phone: 509-372-6227; fax: 509-371-7344; e-mail: Wooyong.um@pnnl.gov.

Notes

The authors declare no competing financial interest.

ACKNOWLEDGMENTS

This research was supported by the U.S. Department of Energy's (DOE) Waste Treatment and Immobilization Plant Project of the Office of River Protection. This research was performed using PNNL Institutional Computing at Pacific Northwest National Laboratory. We gratefully acknowledge T.S. Carlson, K.R. Glaesemann for computational support and E. Kim for guidance and discussion.

REFERENCES

- (1) Choppin, G.; Liljenzin, J.-O.; Rydberg, J. *Radiochemistry and Nuclear Chemistry*. Butterworth-Heinemann: Woburn, MA, 2002.
- (2) Li, D.; Kaplan, D. I. Sorption coefficients and molecular mechanisms of Pu, U, Np, Am and Tc to Fe (hydr)oxides: A review. *J. Hazard. Mater.* **2012**, *243*, 1–18.
- (3) Lieser, K. H.; Bauscher, C. Technetium in the hydrosphere and in the geosphere I. Chemistry of technetium and iron in natural waters and influence of the redox potential on the sorption of technetium. *Radiochim. Acta* **1987**, *42*, 205–213.
- (4) Meyer, R. E.; Arnold, W. D.; Case, F. I.; O'Kelley, G. D. Solubilities of Tc(IV) oxides. *Radiochim. Acta* **1991**, *55* (1), 11–18.
- (5) Gephart, R. E. A short history of waste management at the Hanford Site. *Phys. Chem. Earth* **2010**, *35*, 298–306.
- (6) McCloy, J. S.; Riley, B. J.; Goel, A.; Liezers, M.; Schweiger, M. J.; Rodriguez, C. P.; Hrma, P.; Kim, D.-S.; Lukens, W. W.; Kruger, A. A. Rhenium solubility in borosilicate nuclear waste glass: Implications for the processing and immobilization of technetium-99. *Environ. Sci. Technol.* **2012**, *46*, 12616–12622.
- (7) Dzade, N. Y.; Roland, A.; de Leeuw, N. H. A density functional theory study of the adsorption of benzene on hematite (α -Fe₂O₃) surfaces. *Minerals* **2014**, *4*, 89–115.
- (8) Um, W.; Chang, H.-S.; Icenhower, J. P.; Lukens, W. W.; Serne, R. J.; Qafoku, N. P.; Westik, J. H. J.; Buck, E. C.; Smith, S. C. Immobilization of 99-technetium (VII) by Fe(II)-goethite and limited reoxidation. *Environ. Sci. Technol.* **2011**, *45*, 4904–4913.
- (9) Um, W.; Chang, H.-S.; Icenhower, J. P.; Lukens, W. W.; Serne, R. J.; Qafoku, N. P.; Kukkadapu, R. K.; Westik, J. H. J. Iron oxide waste form for stabilizing ⁹⁹Tc. *J. Nucl. Mater.* **2012**, *429*, 201–209.
- (10) McBeth, J. M.; Lloyd, J. R.; Law, G. T. W.; Livens, F. R.; Burke, I. T.; Morris, K. Redox interactions of technetium with iron-bearing minerals. *Mineral. Mag.* **2011**, *75* (4), 2419–2430.
- (11) Marshall, T. A.; Morris, K.; Law, G. T. W.; Mosselmans, J. F. W.; Bots, P.; Parry, S. A.; Shaw, S. Incorporation and retention of 99-Tc(IV) in magnetite under high pH conditions. *Environ. Sci. Technol.* **2014**, *48*, 11853–11862.
- (12) Luksic, S. A.; Riley, B. J.; Schweiger, M. J.; Hrma, P. Incorporating technetium in minerals and other solids: A review. *J. Nucl. Mater.* **2015**, *466*, 526–538.
- (13) Hrma, P.; Crum, J. V.; Bredt, P. R.; Greenwood, L. R.; Arey, B. W.; Smith, H. D. Vitrification and testing of a Hanford high-level waste sample. Part 2: Phase identification and waste form leachability. *J. Nucl. Mater.* **2005**, *345*, 31–40.
- (14) Akatov, A. A.; Nikonov, B. S.; Omel'yanenko, B. I.; Stefanovsky, S. V.; Marra, J. C. Structure of borosilicate glassy materials with high concentrations of sodium, iron, and aluminum oxides. *Glass Phys. Chem.* **2009**, *35* (3), 245–259.
- (15) Akatov, A. A.; Nikonov, B. S.; Omel'yanenko, B. I.; Stefanovskaya, O. I.; Stefanovsky, S. V.; Suntsov, D. Y.; Marra, J. C. Influence of the content of a surrogate of iron aluminite high-level wastes on the phase composition and structure of glassy materials for their immobilization. *Glass Phys. Chem.* **2010**, *36* (1), 45–52.
- (16) Duff, M. C.; Coughlin, J. U.; Hunter, D. B. Uranium coprecipitation with iron oxide minerals. *Geochim. Cosmochim. Acta* **2002**, *66* (20), 3533–3547.
- (17) Dodge, C. J.; Francis, A. J.; Gillow, J. B.; Halada, G. P.; Eng, C.; Clayton, C. R. Association of uranium with iron oxides typically formed on corroding steel surfaces. *Environ. Sci. Technol.* **2002**, *36*, 3504–3511.
- (18) Skomurski, F. N.; Rosso, K. M.; Krupka, K. M.; McGrail, B. P. Technetium incorporation into hematite (α -Fe₂O₃). *Environ. Sci. Technol.* **2010a**, *44*, 5855–5861.
- (19) Skomurski, F. N.; Ilton, E. S.; Engelhard, M. H.; Arey, B. W.; Rosso, K. M. Heterogeneous reduction of U⁶⁺ by structural Fe²⁺ from theory and experiment. *Geochim. Cosmochim. Acta* **2011**, *75*, 7277–7290.
- (20) Brownfield, M. E.; Affolter, R. H.; Stricker, G. D.; Hildebrand, R. T. High chromium contents in Tertiary coal deposits of northwestern Washington - a key to their depositional history. *Int. J. Coal Geol.* **1995**, *27*, 153–169.
- (21) de Waal, S. A. Nickel mineral from Barberton, South Africa: I. Ferroan trevorite. *Am. Mineral.* **1969**, *54*, 1204–1208.
- (22) Lanteigne, S.; Schindler, M.; McDonald, A. M.; Skeries, K.; Abdu, Y.; Mantha, N. M.; Murayama, M.; Hawthorne, F. C.; Hochella, J. F. J. Mineralogy and weathering of smelter-derived spherical particles in soils: Implications for the mobility of Ni and Cu in the surficial environment. *Water, Air, Soil Pollut.* **2012**, *223*, 3619–3641.
- (23) Andersson, D. A.; Stanek, C. R. Mixing and non-stoichiometry in Fe-Ni-Cr-Zn-O spinel compounds: density functional theory calculations. *Phys. Chem. Chem. Phys.* **2013**, *15*, 15550–15564.
- (24) Xu, K.; Hrma, P.; Um, W.; Heo, J. Iron phosphate glass for immobilization of ⁹⁹Tc. *J. Nucl. Mater.* **2013**, *441*, 262–266.
- (25) Pati, S. S.; Gopinath, S.; Panneerselvam, G.; Antony, M. P.; Philp, J. High temperature phase transformation studies in magnetite nanoparticles doped with Co²⁺ ion. *J. Appl. Phys.* **2012**, *112*, 054320–1–9.
- (26) O'Neill, H. S. C.; Navrotsky, A. Simple spinels: crystallographic parameters, cation radii, lattice energies, and cation distribution. *Am. Mineral.* **1983**, *68*, 181–194.
- (27) Bosusquet-Berthelin, C.; Chaumont, D.; Stuerger, D. Flash microwave synthesis of trevorite nanoparticles. *J. Solid State Chem.* **2008**, *181*, 616–622.
- (28) Fleet, M. E. The structure of magnetite. *Acta Crystallogr., Sect. B: Struct. Crystallogr. Cryst. Chem.* **1981**, *B37*, 917–920.
- (29) Gorter, E. W. Saturation magnetization and crystal chemistry of ferromagnetic oxides. *Philips Research Reports* **1954**, *9*, 295–365.
- (30) Shannon, R. D. Revised effective ionic radii and systematic studies of interatomic distances in halides and chalcogenides. *Acta Crystallogr., Sect. A: Cryst. Phys., Diffr., Theor. Gen. Crystallogr.* **1976**, *A32*, 751–767.
- (31) Peretyazhko, T. S.; Zachara, J. M.; Kukkadapu, R. K.; Heald, S. M.; Kutnyakov, I. V.; Resch, C. T.; Arey, B. W.; Wang, C. M.; Kovarik, L.; Phillips, J. L.; Moore, D. A. Pertechetate (TcO₄⁻) reduction by reactive ferrous iron forms in naturally anoxic, redox transition zone sediments from the Hanford Site, USA. *Geochim. Cosmochim. Acta* **2012**, *92*, 48–66.
- (32) Peretyazhko, T.; Zachara, J. M.; Heald, S. M.; Jeon, B.-H.; Kukkadapu, R. K.; Liu, C.; Moore, D.; Resch, C. T. Heterogeneous reduction of Tc(VII) by Fe(II) at the solid-water interface. *Geochim. Cosmochim. Acta* **2008a**, *72*, 1521–1539.
- (33) Liu, J.; Pearce, C. I.; Qafoku, O.; Arenholz, E.; Heald, S. M.; Rosso, K. M. Tc(VII) reduction kinetics by titanomagnetite (Fe_{3-x}Ti_xO₄) nanoparticles. *Geochim. Cosmochim. Acta* **2012**, *92*, 67–81.
- (34) Heald, S. M.; Krupka, K. M.; Brown, C. F. Incorporation of pertechetate and perrhenate into corroded steel surfaces studied by X-ray absorption fine structure spectroscopy. *Radiochim. Acta* **2012**, *100*, 243–253.
- (35) Dovesi, R.; Saunderson, V. R.; Roettie, C.; Orlando, R.; Zicovich-Wilson, C. M.; Pascale, F.; Civalleri, B.; Doll, K.; Harrison, N. M.; Bush, I. J.; D'Arco, P.; Llunell, M.; Causà, M.; Noël, Y. *CRYSTAL14 User's Manual*, Torino, 2014.
- (36) Smith, F. N.; Taylor, C. D.; Um, W.; Kruger, A. A. Technetium incorporation into goethite (α -FeOOH): An atomic-scale investigation. *Environ. Sci. Technol.* **2015**, *49* (22), 13699–13707.

- (37) Iordanova, N.; Dupuis, M.; Rosso, K. M. Charge transport in metal oxides: A theoretical study of hematite α -Fe₂O₃. *J. Chem. Phys.* **2005**, *122*, 144305–1–10.
- (38) Rosso, K. M.; Smith, D. M.; Dupuis, M. An ab initio model of electron transport in hematite (α -Fe₂O₃) basal planes. *J. Chem. Phys.* **2003**, *118* (14), 6455–6466.
- (39) Skomurski, F. N.; Kerisit, S.; Rosso, K. M. Structure, charge distribution, and electron hopping dynamics in magnetite (Fe₃O₄) (100) surfaces from first principles. *Geochim. Cosmochim. Acta* **2010b**, *74*, 4234–4248.
- (40) Freyria Fava, F. Laurea Thesis, Torino University, Torino, Italy, 1995.
- (41) Hohenberg, P.; Kohn, W. Inhomogeneous electron gas. *Phys. Rev.* **1964**, *136* (3B), B864–B871.
- (42) Kohn, W.; Sham, L. J. Self-consistent equations including exchange and correlation effects. *Phys. Rev.* **1965**, *140* (4A), A1133–A1138.
- (43) Mulliken, R. S. Electronic populations analysis on LCAO-MO molecular wave functions. I. *J. Chem. Phys.* **1955**, *23* (10), 1833–1840.
- (44) Verwey, E. J. W. Electronic conduction of magnetite (Fe₃O₄) and its transition point at low temperatures. *Nature* **1939**, *144* (3642), 327–328.
- (45) Rekhila, G.; Bessekhoud, Y.; Trari, M. Visible light hydrogen production on the novel ferrite NiFe₂O₄. *Int. J. Hydrogen Energy* **2013**, *38*, 6335–6343.
- (46) Shuller-Nickles, L. C.; Bender, W. M.; Walker, S. M.; Becker, U. Quantum-mechanical methods for quantifying incorporation of contaminants in proximal minerals. *Minerals* **2014**, *4*, 690–715.
- (47) Rodriguez, E. E.; Poineau, F.; Llobet, A.; Sattelberger, A. P.; Bhattacharjee, J.; Waghmare, U. V.; Hartmann, T.; Cheetham, A. K. Structural studies of TcO₂ by neutron powder diffraction and first-principles calculations. *J. Am. Chem. Soc.* **2007**, *129*, 10244–10248.
- (48) Deutsch, W. J.; Cantrell, K. J.; Krupka, K. M.; Lindberg, M. L.; Serne, R. J. Hanford tank residual waste - Contaminant source terms and release models. *Appl. Geochem.* **2011**, *26*, 1681–1693.
- (49) Navrotsky, A. *Physics and Chemistry of Earth Materials*; Cambridge University Press: New York, NY, 1994; p 417.
- (50) Cornell, R. M.; Schwertmann, U. *The Iron Oxides: Structure, Properties, Reactions, Occurrences and Uses*, 2nd ed.; Wiley-VCH Verlag GmbH & Co: KGaA Weinheim, FRG, 2003.
- (51) Gorski, C. A.; Handler, R. M.; Beard, B. L.; Pasakarnis, T.; Johnson, C. M.; Scherer, M. M. Fe atom exchange between aqueous Fe²⁺ and magnetite. *Environ. Sci. Technol.* **2012**, *46*, 12399–12407.
- (52) Handler, R. M.; Beard, B. L.; Johnson, C. M.; Scherer, M. M. Atom exchange between aqueous Fe(II) and goethite: An Fe isotope tracer study. *Environ. Sci. Technol.* **2009**, *43*, 1102–1107.
- (53) Beard, B. L.; Handler, R. M.; Scherer, M. M.; Wu, L.; Czaja, A. D.; Heimann, A.; Johnson, C. M. Iron isotope fractionation between aqueous ferrous iron and goethite. *Earth Planet. Sci. Lett.* **2010**, *295*, 241–250.
- (54) Yanina, S. V.; Rosso, K. M. Linked reactivity at mineral-water interfaces through bulk crystal conduction. *Science* **2008**, *320*, 218–222.
- (55) Greaves, C. A powder neutron diffraction of vacancy ordering and covalence in γ -Fe₂O₃. *J. Solid State Chem.* **1983**, *49*, 325–333.
- (56) Gualtieri, A. F.; Venturelli, P. In situ study of the goethite-hematite phase transformation by real time synchrotron powder diffraction. *Am. Mineral.* **1999**, *84*, 895–904.
- (57) Droubay, T.; Rosso, K. M.; Heald, S. M.; McCready, D. E.; Wang, C. M.; Chambers, S. A. Structure, magnetism, and conductivity in epitaxial Ti-doped α -Fe₂O₃ hematite: Experiment and density functional theory calculations. *Phys. Rev. B: Condens. Matter Mater. Phys.* **2007**, *75*, 104412–1–7.
- (58) Pearce, C. I.; Qafoku, O.; Liu, J.; Arenholz, E.; Heald, S. M.; Kukkadapu, R. K.; Gorski, C. A.; Henderson, C. M. B.; Rosso, K. M. Synthesis and properties of titanomagnetite (Fe_{3-x}Ti_xO₄) nanoparticles: A tunable solid-state Fe(II/III) redox system. *J. Colloid Interface Sci.* **2012**, *387*, 24–38.
- (59) Pearce, C. I.; Liu, J.; Baer, D. R.; Qafoku, O.; Heald, S. M.; Arenholz, E.; Grosz, A. E.; McKinley, J. P.; Resch, C. T.; Bowden, M. E.; Engelhard, M. H.; Rosso, K. M. Characterization of natural titanomagnetites (Fe_{3-x}Ti_xO₄) for studying the heterogeneous electron transfer to Tc(VII) in the Hanford subsurface. *Geochim. Cosmochim. Acta* **2014**, *128*, 114–127.
- (60) Berry, F. J.; Greaves, C.; Helgason, Ö.; McManus, J. Synthesis and characterization of tin-doped iron oxides. *J. Mater. Chem.* **1999**, *9*, 223–226.